Progress In Electromagnetics Research B, Vol. 55, 115–130, 2013

MICROWAVE BREAST SCREENING IN THE TIME-DOMAIN: IDENTIFICATION AND COMPENSATION OF MEASUREMENT-INDUCED UNCERTANTIES

Emily Porter*, Evgeny Kirshin, Adam Santorelli, and Milica Popović

Department of Electrical and Computer Engineering, McConnell Building, McGill University, 3480 University, Montreal H3A 0E9, Canada

Abstract—In this work we examine several sources of measurement uncertainty that can hinder the use of time-domain microwave techniques for breast imaging. The effects that are investigated include those due to clock and trigger jitter, antenna movements, discrepancies in antenna fabrication, and random measurement noise. We explore the significance of the noise contribution of each effect, and present methods to mitigate them when possible and necessary. We demonstrate that, after applying the aforementioned methods, the noise is minimized to the noise floor of the system, thereby enabling successful tumor detection.

1. INTRODUCTION

Microwave techniques for breast cancer screening and detection have been heavily researched over the past decade. These methods have the potential to be used as a complementary modality to the current standard for breast imaging, x-ray mammography. Microwave imaging has the potential to offer several advantages, including low-cost and comfortable scans; it also does not use the ionizing radiation that mammography requires. Several experimental microwave breast imaging systems have been demonstrated in the literature, most of which operate based on measurements in the frequency domain [1–5]. However, a system that performs measurements in the time domain could be advantageous in terms of improved cost-effectiveness

Received 22 August 2013, Accepted 23 September 2013, Scheduled 24 September 2013
* Corresponding author: Emily Porter (emily.porter@mail.mcgill.ca).

and faster signal recording time [6]. Investigation into experimental time-domain breast imaging has been limited, with few developed systems appearing in the literature [6–8]. For this reason, we choose to explore the potential of time-domain breast cancer screening. Our imaging system, a multistatic radar setup [8], utilizes time-domain measurements with a 16-element antenna array and has been thoroughly tested on breast phantoms.

Radar systems using time-domain measurements frequently aim not to reconstruct a dielectric profile of the breast but rather to identify the most prominent scatterers of electromagnetic energy (i.e., tumor tissues). In particular, our system and many other studies involving time-domain simulations or measurements [7–10] use variations of the differential [9] or baseline [8, 10] method in order to help identify tumors. These methods require using previous breast scans as a comparison basis for the new breast scan data; the presence of malignant tissues is deduced from the changes between the scans. This method can be highly susceptible to measurement inconsistencies. For instance, if all aspects of the measurement are not held constant between the two scans it is possible that the signature of malignant tissues may be embedded within the introduced noise. While we are aware of no literature that addresses this particular issue in microwave radar time-domain breast screening, studies were reported on related issues with microwave tomography: in [3], the authors investigate the error due to sensor and cable movements in their prototype system, and numerical simulations are used to determine the robustness of given imaging algorithms to noise in [11, 12]. In our imaging system, we have identified several sources of discrepancy (hereafter referred to just as "noise") in the measurement data between scans performed at different times. These include equipment-generated uncertainties, such as clock jitter, as well as mechanical issues like antenna movement between scans. In this work, we determine which of the noise sources have the greatest impact on the effective application of the differential method; furthermore, we demonstrate how to mitigate the associated undesirable effects in order to successfully extract the tumor signature from the recorded data.

2. MEASUREMENT DESCRIPTION

The aim of our breast cancer screening system is to identify the presence of malignancies in the breast at an early stage of growth when treatment would be the most successful. We propose to do this by frequent monitoring; a patient would undergo regular microwave breast scans at prescribed intervals. The current and past scans

can then be compared to determine if there are any irregularities in the breast tissue. Following detection of an abnormality with microwave screening, the presence of a breast tumor can be confirmed using traditional technologies (for instance, mammography or magnetic resonance imaging). The feasibility of monitoring the breast via comparison of scans from different times was shown numerically in [9].

Our time-domain microwave breast screening system has been described in detail in [8]. The system incorporates an antenna array held in the exterior surface of a hemispherical bowl-shaped radome. The radome is made from Alumina ($\varepsilon_r = 9.6$), with the relative permittivity chosen to optimize the performance of the antenna according to its design reported in [13]. The breast to be scanned is positioned in the bowl of the radome, with a gel-like material filling any gaps between the radome wall and the skin surface. The selected lossy material is ultrasound gel; a description and detailed motivation for using this medium can be found in [8].

The antenna array contains 16 Travelling-Wave Tapered and Loaded Transmission-Line Antennas (TWTLTLA) [13]. The end-fire antennas are held in slots along the exterior of the radome (our current method of fixing the antennas is described in further detail in Subsection 4.1). The system operates as follows. A specially shaped pulse with frequency content concentrated in the 2–4 GHz range as in [14] is generated on the rising edge of each clock period (clock frequency = 25 MHz) using a Synthesized Broadband Reflector (SBR [14]). This pulse passes through an amplifier (2–8 GHz operating range, +35 dB gain, maximum output power 33 dBm) and is fed into an automated switching matrix that selects a transmitting antenna. The 16×2 switching matrix connects all 16 antennas to input (transmitter) and output (receiver) paths in turn. Finally, the selected receive antenna picks up the signal scattered off the breast. A sampling oscilloscope (pico Technologies, PicoScope 9201) using an equivalent-time sampling rate of 80 GSa/s (i.e., with a 12.5 ps sampling period) records the data. Each recording contains 2 channels: the received signals (Channel 2) and the reference clock signal (Channel 1). A total of 240 bistatic signals are obtained. A photograph of the radome, antenna array, and switching matrix; along with a close-up of the antenna, is provided in Figure 1.

The breast phantom used in this series of tests is a homogeneous fat-mimicking phantom, made of an oil and gelatin mixture. Details on the phantom fabrication and dielectric property measurements can be found in [15, 16], respectively. The fat phantom has a relative permittivity, ε_r, of 10 (± 2), [15, 16]. As phantom properties vary slightly between fabrications, all measurements presented here have

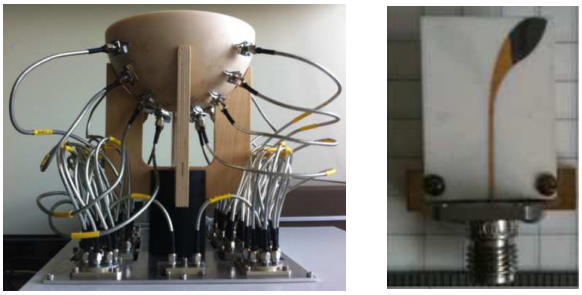

(a) (b)

Figure 1. (a) The radome, antenna array, and switching matrix; and (b) the TWTLWLA antenna.

been conducted on the same phantom in order to eliminate this as a possible source of noise. We instead focus our study on noise sources that are inherent to the system itself.

Once a set of measurements has been recorded, the data is processed using the differential method. This method requires taking two breast scans from the same patient, at different times. If there is a significant change in the scan result between the scan times, this is an indication that there could be abnormal tissue growth within the breast. In order to make such a comparison, signals from corresponding antenna-pairs in both data sets must be aligned and subtracted. As will be seen in the next section, several sources of horizontal noise and measurement uncertainty affect how well we can perform the subtraction.

3. CAUSES OF MEASUREMENT NOISE

This section will describe contributing factors to measurement uncertainties and other noise sources that occur in our system between breast scans.

3.1. Antenna Effects

Two sources of uncertainty in measurements exist due to the antennas and their interaction with the system. These include: antenna movements with respect to each other or the radome in between scans and small differences in antenna fabrication that result in varying performance between antennas. Antenna movement can be a significant issue because changing the position or orientation of the

antennas between scans can lead to different paths travelled for both transmitted and scattered waves. This results in changes in phase and attenuation, which thereby affect the collected signals. Thus, it can be a source of both horizontal and vertical noise. Good repeatability in the positioning of antennas was also seen in [3] to be an important factor in reproducing results between scans. Further, inconsistencies in antenna fabrication alter the transmission and reflection coefficients of the antenna-pairs. Such inconsistencies are mainly due to the antenna feed, which requires soldering of an SMA (SubMiniature version A) connector onto the metallized feeding strip of the antenna. The strip has a width of only 375 µm, making it difficult to achieve accurate and repeatable soldering. The differences in solder lead to variations in feed efficiency, which thereby affect the reflection coefficient (S_{11}) of the antenna.

3.2. Jitter Effects

Jitter, i.e., inconsistent deviations in the timing of signals, occurs in both the reference clock signal and the trigger of the oscilloscope. However, as only the compound effect of these two clock jitters can be viewed on the oscilloscope, we consider them for the purposes of this discussion to be a single source of horizontal noise. The clock jitter causes misalignment between subsequent time-domain recordings and channels on the oscilloscope; this effect leads to difficulties in both applying differential methods that require the subtraction of signals recorded at two different instances and in focusing for imaging algorithms. In order to identify the changes in breast composition between the two scan times, we want to subtract the relevant signals correctly. For this to happen, the recorded signals within each scan must be properly synchronized. Since the oscilloscope triggers recording of the signals, the jitter can cause signal misalignment, and therefore, render their subtraction a meaningless result.

3.3. Random Noise

All collected signals are affected by random noise. This vertical noise from the oscilloscope is particularly undesirable due to the low-level tumor response signals we are attempting to detect. The oscilloscope has a maximum root mean square (RMS) noise of less than 2.5 mV when operating in full bandwidth mode. This value is low; however, the embedded tumor response can be on the same order of magnitude and thus it is beneficial to minimize the noise as much as possible.

4. MITIGATION OF NOISE AND COMPENSATION METHODS FOR UNCERTAINTIES

4.1. Mitigation of Antenna-related Noise

The effects of unintentional antenna movements and differences in antenna fabrication will be detrimental to the repeatability of breast scans, as described in Subsection 3.1. It is therefore essential to minimize these two effects in order to have successful comparison of breast scans over time.

In fact, we can deal with both effects by making one simple adjustment to the system: solidly fix all antennas in place in the radome, without allowing them space to wiggle or to be removed from their enclosures in the radome. This makes any discrepancies in different antennas' S_{11} irrelevant by always using the same antenna in the same position in the radome. In this manner, any irregularities in antenna behavior appear consistently from one breast scan to another, and are therefore removed with subtraction. Fixing the antennas permanently in position also minimizes antenna movement with respect to the radome.

Physically, it is very challenging to hold the antennas permanently in place as the system is designed to be portable and thus components must come apart and be put back together quickly. The antennas must be held sufficiently such that they cannot shift in place when, for instance, someone touches a cable or the radome; however, they must also be removable for inspection and updates to the system. After much trial and error and testing, this has led us to design a "suitcase" that can securely hold the antenna in place in the radome: it has two halves, a hollowed out lower half that is sized precisely to fit the antenna, and a solid upper half that fills the remaining gap between the antenna and the radome in the slot. The upper portion has a

(a) (b)

Figure 2. (a) Top and bottom halves of the "suitcase", and (b) the antennas held in place in the radome using the suitcases.

tag that allows us to gently pull the antenna out of the slot. The suitcases are made of Eccostock HiK (Emerson & Cuming, $K = 10$), a dielectric material with properties very similar to that of the radome. Photographs of a suitcase and suitcases holding antennas in the radome are shown in Figure 2.

4.2. Compensation for Jitter

To compensate for the effects of jitter on the signals collected by our system, we investigate two possible methods. The first method, called "reference alignment," involves recording the clock signal (at Channel 1 of the oscilloscope) that is the trigger for the generated impulse. Then, we align the received signals (recorded at Channel 2) from different scans in the time-domain based on the phase differences in the recorded clock. The second method, called "correlation alignment," aligns signals by identifying the time shift that leads to the best match between the signals. Descriptions of these techniques are provided in the following paragraphs.

For both techniques, we assume that two complete data sets have been recorded at different times but from the same patient. Each set contains 240 signals, and each of the 240 signals corresponds to another signal in the other set. For example, in Set #1, the signal received at antenna y when antenna x was transmitting can be denoted as $S^1_{x,y}$. This corresponds to the signal from the same transmit/receive antenna pair (x, y) in Set #2: $S^2_{x,y}$. We call Set #1, the initial breast scan, the "baseline" data. Note that data is always compared between antenna pairs, i.e., between transmit and receive antennas that are located in the radome in the same position for both scans. If the breast composition was the same at the time of scanning Set #1 and #2, then (neglecting noise and measurement uncertainties),

$$S^1_{x,y} = S^2_{x,y}. \tag{1}$$

However, if the breast composition had changed such that Set #2 was collected when a tumor was present, then,

$$S^2_{x,y} = S^1_{x,y} + T_{x,y}, \tag{2}$$

where $T_{x,y}$ is the tumor response for antenna pair (x, y), and

$$x, y \in \{1, \ldots, 16\}, \quad y \neq x. \tag{3}$$

However, in practice, the signals $S^1_{x,y}$ and $S^2_{x,y}$ cannot be directly subtracted to determine if there is a significant $T_{x,y}$ because of the jitter in the trigger clock. For successful subtraction, the signals must first be time-aligned. Further, since the pulse has a short-duration (70 ps full-width at half-maximum at the output of the pulse generator),

slight misalignments can seriously degrade the quality of the resulting subtraction. This underscores the need for a compensation method that can align data from the two sets to a fine resolution in time.

Reference alignment is performed by analyzing the signals recorded at Channel 1 of the oscilloscope. This channel records the clock, i.e., "reference" signal. Channel 2, on the other hand, records the received signal from the system. As shown in Figure 3, we find the relative delay between two reference signals, one each from Set #1 and Set #2, for the same x and y. This relative time-shift is denoted as ΔT (sub-sample values are possible if interpolation is used). We then shift the signal from S^2 recorded at Channel 2 accordingly, to compensate ΔT so that the S^1 and S^2 signals are aligned in time. We assume that ΔT is equal over the oscilloscope channels up to the cross-channel jitter (< 3.5 ps RMS, according to the specifications). At this stage the two signals are aligned and the subtraction can take place.

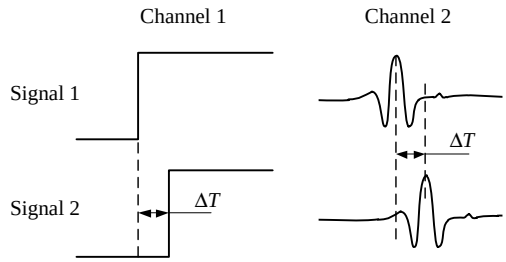

Figure 3. Schematic illustrating the procedure of reference time-alignment: delay associated with jitter between two signals recorded at Channel 2 is determined from the auxiliary "reference" signals recorded at Channel 1, where Signal 1 is from S^1 and Signal 2 is from S^2 for a given x and y.

In *correlation alignment*, ΔT is found only from signals recorded at Channel 2 by computing the maximum cross-correlation between the signals to find the best match. In other words, it takes only received signal data (no reference signal) for $S^1_{x,y}$ and $S^2_{x,y}$ for each x, y combination and finds the amount of time-shift of $S^2_{x,y}$ required such that it overlaps maximally with $S^1_{x,y}$. This technique is applicable only for calibration purposes or when two scans are available, for example, to subtract a baseline signal from a signal with a tumor response from the same antenna pair, in order to remove the direct pulse. For imaging based on a single breast scan, the collected signals still require time-alignment; in this case only reference alignment (as described above) is applicable as there are no baseline signals available to enable the use of

correlation alignment (signals within a single breast scan from different antenna pairs cannot be used for correlation alignment purposes as they have varying shapes).

4.3. Compensation for Random Noise

We use averaging to decrease the random noise seen in the received signals. This has the effect of increasing the vertical resolution of the data, and allows signals that are buried below the noise level to potentially be extracted. The oscilloscope offers hardware averaging with the drawback of increased recording time. Our test measurements show that without hardware averaging the noise level is around 12–13 mV, whereas with 32 averages the noise decreases to less than 1.8 mV and with 64 averages to less than 1.5 mV. In our case, we choose to average each signal 32 times, as it provided the best trade-off between measurement time and noise reduction. For our application, the improvement seen with 64 averages as compared to 32 averages is negligible.

5. RESULTS

In order to examine the noise in received signals due to the jitter and antenna effects, we analyze the standard deviation of the measured data. In particular, the standard deviation in received signals over 15 measurements is calculated for each scenario. Signals are recorded with 4096 time samples at an equivalent-time sampling rate of 80 GSa/s. The standard deviation is then calculated across the 15 measurements at each sample time t, such that a vector spanning the entire sampling domain is created. We also present maximum and average standard deviations, which are computed across all 4096 samples.

We first present results for jitter compensation, so that these methods can be applied before examining noise due to the antennas. To see the effect that jitter has on the system, we hold all other variables constant and take 15 measurements in a row for each of two antenna transmit-receive pairs. We then apply both reference and correlation alignment methods to the signals in an attempt to decrease the effects of jitter on the collected data.

Figure 4 shows the standard deviations from the average for received signals from each antenna-pair without any compensation, with reference alignment compensation, and with correlation alignment compensation. We see that without compensation, jitter alone can contribute up to almost 14 mV of noise in the received signals. As

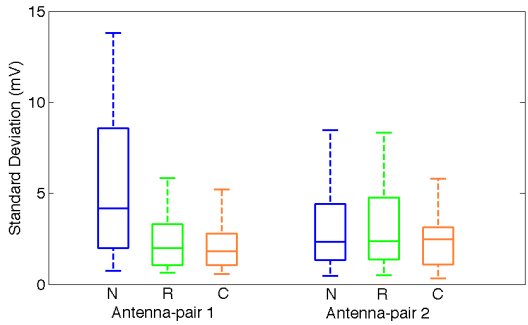

Figure 4. Effects of jitter for two antenna pairs: box plot showing standard deviation quartiles when no compensation is performed (N, blue), after reference alignment (R, green), and after correlation alignment (C, orange). Whiskers show the minimum and maximum standard deviation values while the box limits mark the 25th (lower) and 75th (upper) percentiles and the horizontal line dividing each box is the median standard deviation.

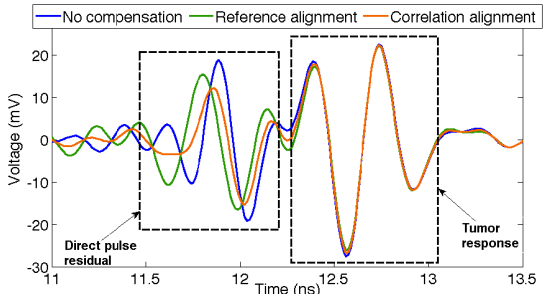

Figure 5. Differential signals obtained using the two alignment methods, compared to without any alignment. It can be seen that alignment helps provide suppression of the direct pulse.

the tumor signature embedded in received signals is typically on the order of tens of millivolts [8, 14], this amplitude of jitter in the signal could obscure relevant information regarding the tumor. Correlation alignment and reference alignment are both successful in decreasing the effects of jitter. In particular, after correlation alignment is applied, the noise due to jitter seen in the received signals is only 2.2 mV on average, which is at the level of the noise floor of the oscilloscope (< 2.5 mV RMS). Figure 5 shows an example of the differential signals for the two alignment types compared to that without time alignment (direct

subtraction). The reference time alignment is not always as efficient as the correlation alignment due to cross-channel trigger jitter, which the correlation alignment accounts for but reference alignment does not.

We examine the contribution of antenna effects on the noise seen in the received signals. In Figures 6–8 we plot the mean, with the standard deviation from this mean shown shaded in red, of the 15 measurements each for cases including random measurement noise, movement of antennas, and the variation due to antenna fabrication irregularities, respectively. This data has been pre-processed by application of the correlation alignment scheme. As seen from Figure 6, the resulting variation in signal amplitude and phase due to random

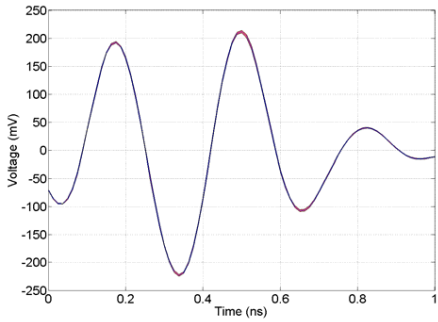

Figure 6. Time-domain signal received with antenna-pair 1 after correlation alignment; standard deviation due to random measurement noise shown shaded in red. In this scenario we see that the signals are consistently aligned such that the standard deviation is at a minimum.

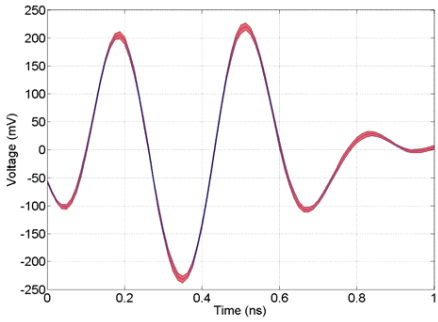

Figure 7. Time-domain signal received with antenna-pair 1 after correlation alignment; standard deviation due to movement of antennas shown shaded in red.

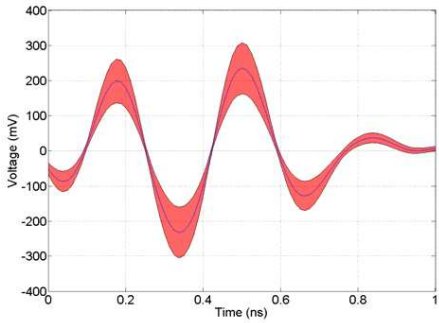

Figure 8. Time-domain signal received with antenna-pair 1 after correlation alignment; standard deviation due to differences in antenna fabrication shown shaded in red.

measurement noise is minimal. When the antennas are moved slightly (within a 2 mm range) at random orientations, the signal deviation as shown in Figure 7 is close to ± 10 mV; whereas the change in received signals found due to discrepancies in antenna fabrication reaches ± 76 mV (Figure 8). These results indicate that the variability in antenna properties (S_{11}) is the most significant source of discrepancy between breast scans, if the antennas are not positioned in the same place for both scans. We note that the analysis of variations in antenna fabrication inherently includes the error from antenna movement as each antenna must be removed from the radome, switched, and then reinserted in order to perform the recording. Further, peak tumor response values for basic heterogeneous phantoms with 1-cm radius malignancies were found to be in the 17 mV–34 mV range in [14], indicating that this response would indeed be obscured without compensation for differences in the fabrication of antennas, especially in the case of more complicated phantoms/smaller tumors.

Table 1 provides a summary of the compensation with standard deviations calculated for each scenario: with random measurement noise only, when antennas are moved, and when antenna fabrication properties are examined. We note that for all of these measurements, the recordings were obtained with 32 averages. This data confirms that holding antennas in place and applying correlation alignment reduces the noise in the received signals of different breast scans due to jitter and antenna effects, to the point where the remaining deviation is near the level of the system's noise floor.

Following compensation for jitter using the correlation method, and fixing the antennas in place to reduce issues related to movement

and fabrication, the standard deviation due to uncertainties and noise is decreased from almost 18% to less than 1% of the peak-to-peak signal strength. Use of the correlation alignment alone can decrease the average standard deviation of the data by up to 60% compared to no alignment, and up to 10% compared to reference alignment.

Finally, to demonstrate how the effect of noise compensation improves reconstructed breast images, we show an example of a 2-D coronal breast slice in Figure 9 produced both without any noise compensation and with compensation. These images have been generated from our experimental data using the Delay-multiply-and-sum (DMAS) algorithm [17] with a voxel size of $2\,\mathrm{mm}^3$. The algorithm generates a 3-D stack of 2-D slices of the breast. For both images, the recorded data set was the same: measurements were taken with a tumor in right hemisphere of the homogeneous breast phantom. In the reconstructed images, red regions represent areas of strongly scattered electromagnetic energy; regions in blue have less scattering. We plot the energy on a linear scale, and note that the global maximum energy (darkest red) should be seen at the tumor location. From the two images, it is clear that without applying any noise compensation the tumor region is not identifiable at all. This is most likely due to the lack of time alignment in between the reflected signals, making it appear as if they originate at different points than they actually do (defeating the objective of the delay-and-sum type algorithms). Once we apply our suggested noise suppression techniques, the reconstructed image localizes the tumor well.

Table 1. Peak (average) standard deviation, for received signals from antenna-pair 1. Standard deviations are listed for uncompensated, reference aligned and correlation aligned signals obtained from random measurement noise, movement of the antennas and examination of differences in antenna fabrication.

	Original	**Reference alignment**	**Correlation alignment**
Random measurement noise (mV)	13.8 (5.2)	5.2 (2.3)	5.2 (2.1)
Moving antennas (mV)	10.7 (6.0)	9.8 (5.7)	8.9 (5.2)
Antenna fabrication (mV)	75.7 (37.6)	76.6 (39.7)	75.5 (32.5)

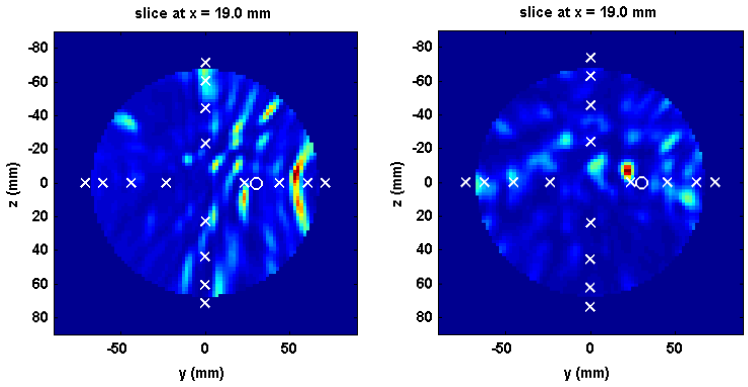

(a) (b)

Figure 9. Reconstructed breast images: 2-D coronal slices at a depth of $x = 19\,\text{mm}$. (a) is the reconstruction generated with no noise compensation; (b) is with compensation. Dark red highlights strong sources of electromagnetic scattering whereas blue represents weak scattering. The "x" markers indicate the positions of the 16 antennas, and the circle notes the actual tumor location. These images show the importance of applying noise compensation to the data, as without it the tumor is not visible.

6. CONCLUSION

In this work we have identified sources of measurement noise in our time-domain microwave cancer detection system that interfere with consistent repeatability of scans. The most significant noise sources included those due to antenna movement, discrepancies in antenna fabrication, and clock jitter. It was found that each of these noise sources must be compensated for in order to reliably detect the low-level tumor response. Methods for mitigation of the noise effects through a combination of both mechanical and software solutions were presented and demonstrated that the inconsistencies between measurements due to noise can be successfully suppressed. In particular, we found that applying time-alignment via correlation to the signals is beneficial in removing the mismatch caused by clock and trigger jitter, and fixing the antennas permanently in place avoids antenna-related noise issues. Implementing these techniques allows for better use of the differential/baseline method in detecting the presence of a tumor and in producing accurate images of the breast.

ACKNOWLEDGMENT

This work was supported by the Natural Sciences and Engineering Research Council of Canada (NSERC), Le Fonds de recherche du Québec — Nature et technologies (FQRNT), and Partenariat de recherche orientée en microélectronique, photonique et télécommunications (PROMPT). The authors are extremely grateful to the McGill University Photonics Systems Group for allowing us use of their lab space and the long-term loan of key measurement components.

REFERENCES

1. Klemm, M., et al., "Development and testing of a 60-element UWB conformal array for breast cancer imaging," *Proceedings of the 5th European Conference on Antennas and Propagation (EUCAP)*, 3077–3079, Rome, Italy, Apr. 11–15, 2011.
2. Meaney, P. M., M. W. Fanning, D. Li, S. Poplack, and K. D. Paulsen, "A clinical prototype for active microwave imaging of the breast," *IEEE Trans. Microw. Theory Techn.*, Vol. 48, No. 11, 1841–1853, Nov. 2000.
3. Bourqui, J., J. M. Sill, and E. C. Fear, "A prototype system for measuring microwave frequency reflections from the breast," *Int. J. Biomedical Imaging*, Vol. 2012, Article ID 851234, 12 Pages, 2012.
4. Li, X., E. J. Bond, B. D. Van Veen, and S. C. Hagness, "An overview of ultra-wideband microwave imaging via space-time beamforming for early-stage breast-cancer detection," *IEEE Antennas Propag. Mag.*, Vol. 47, No. 1, 19–34, Feb. 2005.
5. Flores-Tapia, D. and S. Pistorius, "Real time breast microwave radar image reconstruction using circular holography: A study of experimental feasibility," *Med. Phys.*, Vol. 38, No. 10, 5420–5431, Oct. 2011.
6. Zeng, X., A. Fhager, P. Linner, M. Persson, and H. Zirath, "Experimental investigation of the accuracy of an ultrawideband time-domain microwave-tomographic system," *IEEE Trans. Instrum. Meas.*, Vol. 60, No. 12, 3939–3949, Dec. 2011.
7. Lai, J. C. Y., C. B. Soh, E. Gunawan, and K. S. Low, "UWB microwave imaging for breast cancer detection — Experimentals with heterogeneous breast phantoms," *Progress In Electromagnetics Research M*, Vol. 16, 19–29, 2011.
8. Porter, E., E. Kirshin, A. Santorelli, M. Coates, and M. Popović, "Time-domain multistatic radar system for microwave breast

screening," *IEEE Antennas Wireless Propag. Lett.*, Vol. 12, 229–232, 2013.

9. Byrne, D., M. O'Halloran, M. Glavin, and E. Jones, "Breast cancer detection based on differential ultrawideband microwave radar," *Progress In Electromagnetics Research M*, Vol. 20, 231–242, 2011.
10. Liu, X., X. Xiao, Z. Fan, and J. Yu, "Study on the imaging resolution of ultra-wideband microwave imaging for breast cancer detection," *Proceedings of the 3rd International Conference on Bioinformatics and Biomedical Engineering (ICBBE)*, 1–4, Beijing, China, Jun. 11–13, 2009.
11. Sabouni, A. and S. Noghanian, "The robustness of HGA/FDTD in the presence of noise for microwave breast cancer," *IEEE Antennas and Propagation Society International Symposium (APSURSI)*, 1–4, Charleston, SC, United States, Jun. 1–5, 2009.
12. Zeng, X., A. Fhager, and M. Persson, "Effects of noise on tomographic breast imaging," *General Assembly and Scientific Symposium (URSI)*, 1–4, Istanbul, Turkey, Aug. 13–20, 2011.
13. Kanj, H. and M. Popovi, "A novel ultra-compact broadband antenna for microwave breast tumor detection," *Progress In Electromagnetics Research*, Vol. 86, 169–198, 2008.
14. Santorelli, A., et al., "Experimental demonstration of pulse shaping for time-domain microwave breast imaging," *Progress In Electromagnetics Research*, Vol. 133, 309–329, 2013.
15. Porter, E., J. Fakhoury, R. Oprisor, M. Coates, and M. Popović, "Improved tissue phantoms for experimental validation of microwave breast cancer detection," *Proceedings of the 4th European Conference on Antennas and Propagation (EUCAP)*, 1–5, Barcelona, Spain, Apr. 12–16, 2010.
16. Santorelli, A., "Breast screening with custom-shaped pulsed microwaves," M. Eng. Thesis, Dept. Elec. and Comp. Eng., McGill Univ., Montréal, Canada, 2012.
17. Lim, H. B., N. T. T. Nhung, E. P. Li, and N. D. Thang, "Confocal microwave imaging for breast cancer detection: Delay-multiply-and-sum image reconstruction algorithm," *IEEE Trans. Biomed. Eng.*, Vol. 55, No. 6, 1697–1704, Jun. 2008.